ACS APPLIED MATERIALS & INTERFACES

www.acsami.org

Research Article

Spatial Confinement as an Effective Strategy for Improving the Catalytic Selectivity in Acetylene Hydrogenation

Qiang Fu,* Fan Wu, Bingxue Wang, Yuxiang Bu, and Claudia Draxl

Cite This: *ACS Appl. Mater. Interfaces* 2020, 12, 39352–39361

Read Online

ACCESS | Metrics & More | Article Recommendations | Supporting Information

ABSTRACT: While control over chemical reactions is largely achieved by altering the intrinsic properties of catalysts, novel strategies are constantly being proposed to improve the catalytic performance in an extrinsic way. Since the fundamental chemical behavior of molecules can remarkably change when their molecular scale is comparable to the size of the space where they are located, creating spatially confined environments around the active sites offers new means of regulating the catalytic processes. We demonstrate through first-principles calculations that acetylene hydrogenation can exhibit significantly improved selectivity within the confined sub-nanospace between two-dimensional (2D) monolayers and the Pd(111) substrate. Upon intercalation of molecules, the lifting and undulation of a 2D monolayer on Pd(111) influence the adsorption energies of intermediates to varying extents, which, in turn, changes the energy profiles of the hydrogenation reactions. Within the confined sub-nanospace, the formation of ethane is always unfavorable, demonstrating effective suppression of the unwanted overhydrogenation. Moreover, the catalytic properties can be further tuned by altering the coverage of the adsorbates as well as strains within the 2D monolayer. Our results also indicate that for improving the selectivity, the strategy of spatial confinement could not be combined with that of single-atom catalysis, since the reactant molecules cannot enter the sub-nanospace due to the too weak adsorbate−substrate interaction. This work sheds new light on designing novel catalysts with extraordinary performance for the selective hydrogenation of acetylene.

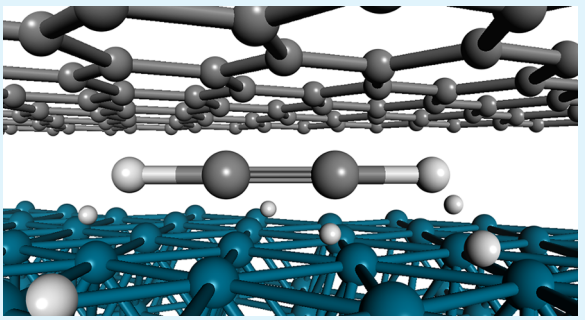

KEYWORDS: *spacial confinement, transition-metal substrate, two-dimensional material, hydrogenation, first-principles simulation, nanoscale*

1. INTRODUCTION

The chemical behavior of molecules can become remarkably distinct once they are confined in volumes that are comparable to their spatial extension. For example, water molecules within the 0.8-nm-diameter carbon nanotube porins adopt a single-file configuration and thus exhibit highly enhanced permeability compared with that of biological water transporters.[1] Moreover, the success of enzymatic reactions greatly benefits from spatial confinement, through which the reactant species are constrained in well-defined spaces around the active sites.[2] Such a type of spatially confined microenvironment—the nanoreactors—can also be created by humans to improve the performance of heterogeneous catalysts. It has been demonstrated that Rh particles confined inside nanotubes exhibit strikingly enhanced catalytic activity for the conversion of CO and H_2 to ethanol,[3,4] and a significant increase in the reaction rate can be achieved once the Pt nanocatalysts are confined inside nanopores.[5] More interestingly, by means of ultraviolet and visible light irradiation, nanoreactors can be reversibly created and destroyed through conversion between an assembled and a disassembled state of nanoparticles, and in this way, the obstacle of reactants entering the confined spaces is overcome.[6] It is obvious that in chemistry, the small spaces of nanoreactors have big implications.[7] As a common feature of the above approaches, control over chemical reactions do not rely on modifying specific catalysts, but instead, rely on tailoring the dimensions of the corresponding microenvironment.[8]

Ethylene (C_2H_4) is widely used in the chemical industry where much of its global production goes toward polyethylene. Unfortunately, the acetylene (C_2H_2) impurity in the industrially produced ethylene feedstock brings about catalyst poisoning and generation of explosive metal acetylides in ethylene polymerization. While the content of the acetylene impurity should be less than a few parts per million (ppm), the actual value in the ethylene feedstock is typically an order of 1%. A preferred approach of reducing the acetylene

Received: July 9, 2020
Accepted: August 6, 2020
Published: August 6, 2020

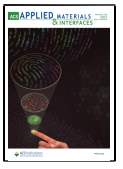

https://dx.doi.org/10.1021/acsami.0c12437
ACS Appl. Mater. Interfaces 2020, 12, 39352–39361

concentration to the acceptable level is to selectively hydrogenate acetylene to ethylene, whereas any overhydrogenation toward ethane (C_2H_6) needs to be inhibited.[9] Pd-based materials are the commonly employed catalysts whose selectivity can be effectively improved by alloying with other elements.[10−13] Meanwhile, alloy catalysts composed of inexpensive transition metals have also been developed.[14,15] Despite the great success, such an alloying strategy is plagued by a few limitations. First, Pd-based alloys cannot completely suppress oligomerizations caused by C−C coupling reactions, which not only compete with acetylene hydrogenation but also deactivate the catalysts.[16,17] Second, the structural flexibility within metal alloys in the reactive environment likely brings about segregation,[18,19] through which the enrichment of Pd in the surface region may cause loss of the desired small Pd ensembles.[20,21] Last but not least, since metals that make up the alloys usually follow similar scaling and Brønsted−Evans−Polanyi (BEP) relations,[22] the overall activities of the alloy catalysts cannot exceed that of the corresponding optimal single-component systems as presented in the volcano-shaped curves.[23,24]

Creating multicomponent catalysts that combine the properties of chemically diverse materials has proven to be a successful way of improving the catalytic performance.[25] One typical application of such a strategy is to construct unique "reaction zones" by depositing surface adsorbates on transition-metal catalysts.[26−32] Through intriguing noncovalent and/or steric interactions between the deposited adsorbates and reactant molecules, the coated transition-metal catalysts can recognize specific molecules or particular adsorption configurations of the reactants and, accordingly, exhibit much-improved selectivity just like enzymes in biological systems.[26,27,31] Two-dimensional (2D) materials like graphene represent another type of adsorbates to form multicomponent catalysts with transition metals. Here, the microenvironment created by covering 2D monolayers on transition-metal surfaces plays the role of not only a sub-nanocontainer for intercalated molecules but also a sub-nanoreactor for reactions between them.[33−35] Especially, the confined spaces in between can bring about the highly enhanced catalytic performance of the transition metals via modulation of the adsorption and reaction properties of the intercalated molecules by these 2D overlayers.[36−41]

The interface composed of one 2D monolayer and a transition-metal surface, which is bonded via van der Waals interactions, usually has an inter-planar spacing of ∼3 Å.[33,34] Upon intercalation of molecules into the sub-nanospace, the 2D monolayer is lifted up and probably deformed, exhibiting undulations. The energy cost for the lifting and deformation can be compensated by molecule−substrate interactions if it is strong enough, and, if the size of the molecules is not too large. Only in this case, the confined sub-nanospace—the microenvironment—can accommodate the molecules. Comparing acetylene, ethylene, and ethane, one can see that their interactions with a transition-metal substrate gradually decrease, whereas the sizes are getting bigger. Thus, the adsorption properties of the three molecules on the transition-metal surface will inevitably be affected, and more importantly, be affected quite differently by the 2D overlayer. Such an impact could also exert on other intermediates in the hydrogenation pathways, like vinyl, ethylidyne, and ethylidene, since the different adsorption configurations that they usually adopt will lead to a disparity in the topography of the 2D monolayer. As such, the adsorption energies of these carbon-containing species will deviate from the intrinsic scaling relation that is established without the presence of graphene. Moreover, the corresponding transition state energies and barriers of the elementary reactions can also be changed to varying degrees under the influence of the 2D overlayer. It is expected that the microenvironment, which can accommodate acetylene but may not be able to hold ethane or multicarbon hydrocarbons formed via oligomerizations, could be an idea reactor for improving the hydrogenation selectivity toward ethylene. In other words, ethylene is expected to be the *only* product of acetylene hydrogenation within the confined microenvironment because the formation of all other molecules will be inhibited both thermodynamically and kinetically.

In this work, systematic first-principles calculations are performed to explore the possibility of employing confined sub-nanospace to improve the hydrogenation selectivity from acetylene to ethylene. The microenvironment is constructed by covering a Pd(111) surface with graphene or a hexagonal boron nitride monolayer. We find that the presence of 2D monolayers exerts different effects on the adsorption properties of the three molecules—acetylene, ethylene, and ethane, and the corresponding energy barriers of the hydrogenation steps are also changed in a similar way. Such effects vary with the coverage of the adsorbates as well as with the strain of the 2D overlayers, and in turn, affect the hydrogenation processes within the sub-nanospace. The formation of the confined microenvironment effectively inhibits the overhydrogenation toward ethane and could promote the conversion from acetylene to ethylene in some cases. Our work opens up a new avenue for improving the catalytic selectivity in acetylene hydrogenation and may shed light on the design and synthesis of novel catalysts with extraordinary performance.

2. COMPUTATIONAL METHODS

2.1. Simulation Model for the Transition-Metal/2D Monolayer Interfaces. In Figure 1, we present the lattice (marked by red solid lines) for both Pd(111) and graphene when constructing the interface model, where the graphene overlayer is placed above the Pd(111) substrate. Here, the corresponding 1 × 1 supercell contains 28 palladium atoms (7 atoms per layer) and 18 carbon atoms. The Pd surface maintains its intrinsic lattice constant, and the graphene overlayer is subjected to a mean compression of 1.28% after being rotated by 19.1°. The choice of such a cell is to achieve a good balance between the strain and the size of the supercell because the

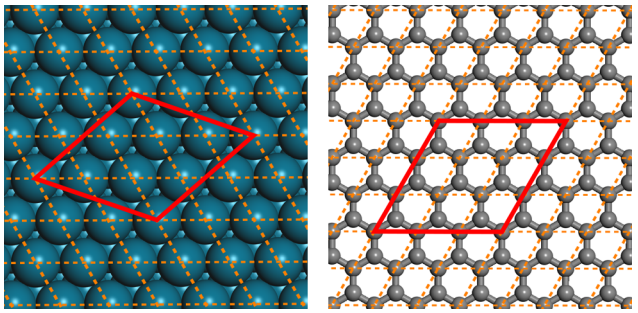

Figure 1. Lattices of the Pd(111) surface and the graphene monolayer in the constructure of the Pd(111)/graphene interface. The corresponding unit cells indicated by red solid lines. The teal blue and gray spheres represent the Pd and C atoms, respectively. The original unit cell of each component is marked by orange dashed lines.

https://dx.doi.org/10.1021/acsami.0c12437
ACS Appl. Mater. Interfaces 2020, 12, 39352−39361

lattices of palladium and graphene are not commensurate. More discussion on this issue can be found in the model construction in ref 42 for a Pt(111)/SnO_2 interface. To create the interface model composed of Pd(111) and hexagonal boron nitride (h-BN), we adopt the same approach and replace two carbon atoms by one boron atom and one nitrogen atom. In this case, the compression applied to the h-BN monolayer increases to 3.04% since the lattice constant of h-BN (2.511 Å) is slightly larger than that of graphene (2.467 Å). Regarding the interface containing a Pd-doped Ag substrate, the lattice of graphene should be matched with that of the hosting Ag(111) surface. Here, the graphene overlayer is subjected to a mean stretch of 1.55%, and the corresponding unit cell is shown in Figure S1. In this interface model, a 1 × 1 supercell contains 24 metal atoms (six atoms per layer) and 16 carbon atoms.

2.2. Computational Details. Our calculations are performed using the Vienna ab initio simulation package (VASP)[43,44] within the framework of density-functional theory (DFT). Plane waves with a cutoff energy of 500 eV are used as basis functions to solve the Kohn−Sham equations. The projector augmented wave (PAW) approach[45] is employed, and the exchange−correlation effects are described by the optB86b-vdW functional,[46−48] which explicitly accounts for van der Waals interactions. The employed computational approach can well describe hydrogenation reactions on transition-metal substrates[13] and chemical reactions within spatially confined microenvironments.[33,34] Regarding the surface and interface systems containing Pd(111), the Brillouin zone (BZ) is sampled using a 5 × 5 × 1 Monkhorst−Pack grid[49] for the 1 × 1 supercell and a 3 × 3 × 1 grid for a larger 2 × 2 supercell. The BZ sampling is performed using comparable *k*-grids for systems that contain the Pd-doped Ag(111) substrate. The slab models that we use to simulate the transition-metal surfaces contain four atomic layers of metals plus a sufficiently thick region of vacuum. Here, the bottom two layers are kept frozen during atomic relaxation, while the coordinates of all other atoms, including those in the adsorbates and the 2D monolayers, are relaxed until the maximum force is less than 0.03 eV/Å. Dipole corrections are applied to avoid spurious interactions between periodic images in the vertical direction. The transition states in the hydrogenation reactions are located using the climbing-image nudged elastic band method[50] with a force criterion of 0.05 eV/Å. The adsorption energy

$$E_{ads} = E_{surf-mol} - (E_{surf} + E_{mol}) \quad (1)$$

is used to describe the interaction strength between transition-metal substrates and adsorbed molecules. Here, E_{surf} and E_{mol} are the energies of the substrates (or the interfaces) and the isolated molecules, respectively, and $E_{surf-mol}$ represents the energy of the combined system upon adsorption. A negative E_{ads} value corresponds to exothermic adsorption.

3. RESULTS AND DISCUSSION

3.1. Interactions Between Pd(111) and the Graphene Overlayer. Upon formation of the Pd(111)/graphene interface, the flat graphene monolayer is located at 3.20 Å above the Pd(111) substrate. For the 1 × 1 supercell (the red lines in Figure 1), the binding energy of the two components is calculated to be −1.46 eV. Without the vdW correction, i.e., using the functional PBE,[51] the value becomes +0.13 eV. Such a comparison indicates that the bonding at the interface mainly comes from van der Waals interactions. In Figure 2, we plot the plane-averaged electrostatic potentials of the Pd(111) substrate (blue dashed line), the graphene overlayer (orange dashed line), and the Pd(111)/graphene interface (black solid line). One can see that while the respective electrostatic potential of Pd(111) and graphene is equal at the two sides of the corresponding system, a step of 1.09 eV appears in the electrostatic potential when the components are combined to form the interface. It demonstrates that upon binding of graphene on Pd(111), redistribution of the charge density

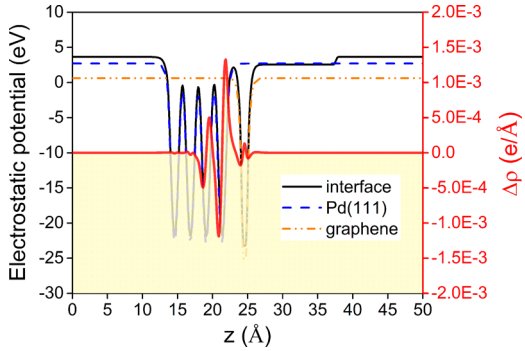

Figure 2. Plane-averaged electrostatic potential (black solid line) and charge density difference (red solid line) of the Pd(111)/graphene interface along the vertical direction. The plane-averaged electrostatic potential of the Pd(111) substrate and the graphene monolayer are shown by blue and orange dashed lines, respectively.

leads to the appearance of an interfacial dipole. However, charge transfer across the interface is extremely small as verified by the Bader charge analysis. It reveals that the charge redistribution at the interface merely brings about polarization, which is also evident from the plane-averaged charge density difference of the interface $\Delta\rho = \rho_{interface} - (\rho_{Pd(111)} + \rho_{graphene})$ (red solid line). Here, $\rho_{Pd(111)}$ and $\rho_{graphene}$ are the corresponding charge density of the two pristine systems, and $\rho_{interface}$ is that of the interface system. The density of states (DOS) of the Pd *d* electrons before and after the deposition of graphene is presented in Figure S2. The very tiny change in the DOS upon formation of the interface demonstrates a negligible influence of the polarization on the electronic structure of the Pd(111) substrate, meaning that the intrinsic catalytic properties of the Pd species do not change. This is different from the case where transition-metal particles are placed within carbon nanotubes.[4]

3.2. Adsorption of C_2H_2, C_2H_4, and C_2H_6 on the Pd(111) Surface and Within the Pd(111)/Graphene-Confined Sub-Nanospace. Our studies on the adsorption properties of C_2H_2, C_2H_4, and C_2H_6 first focus on a particular coverage of the adsorbates, corresponding to one C_2H_x (x = 2, 4, and 6) molecule occupying a 2 × 2 supercell, i.e., one adsorbed molecule corresponds to 28 Pd atoms at the surface layer. Higher coverage will be discussed in the subsequent sections. The adsorption of C_2H_2 and C_2H_4 on Pd(111) was previously investigated in several theoretical studies.[52−55] Five different adsorption structures including one top configuration (π type), one bridge configuration (di-σ type), and three hollow ones (see Figure 1 in ref 54) were considered for C_2H_2 adsorption.[54] As for the hollow sites on Pd(111), here, we do not distinguish hcp or fcc hollow sites, since the difference in the adsorption energies of acetylene was found to be very small.[52,54] In our calculations, we have taken into account all of the five structures and found that one hollow configuration, in which the C−C bond is parallel to the Pd−Pd bond (left panel in Figure 3a), is the most favorable structure, consistent with previous investigations.[52,54] The adsorption energy of such a configuration is calculated to be −2.53 eV, which also agrees well with the previous result of −2.24 eV,[54] considering that the latter does not include contributions of van der Waals interactions. Regarding the adsorption of C_2H_4, two adsorption patterns—the π type and the di-σ type—were previously investigated, with the di-σ configuration (left panel in Figure 3b) being more stable.[53] The same conclusion is obtained in

https://dx.doi.org/10.1021/acsami.0c12437
ACS Appl. Mater. Interfaces 2020, 12, 39352−39361

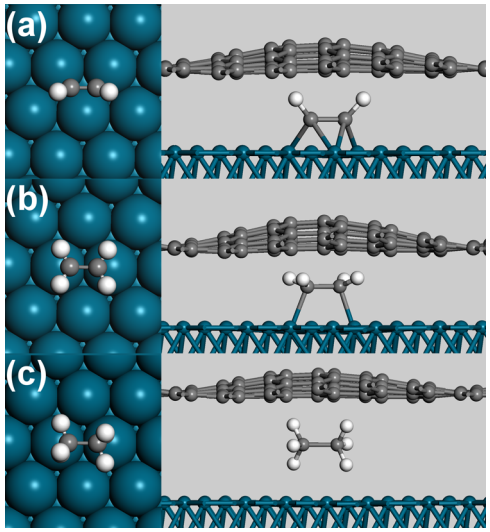

Figure 3. Adsorption structures of C_2H_2 (a), C_2H_4 (b), and C_2H_6 (c) molecules on the bare Pd(111) surface (left panel: top view) and within the sub-nanospace (right panel: side view) between Pd(111) and the graphene overlayer.

our calculations, with the adsorption energy of ethylene being −1.43 eV. For the adsorption of C_2H_6, the adsorption energy is calculated to be −0.40 eV, which is much smaller than the values of C_2H_2 and C_2H_4 adsorbates. This is not surprising since no covalent bond is involved in the interaction between ethane and the substrate but mere van der Waals interactions (left panel in Figure 3c).

Upon covering the Pd(111) surface by graphene, the adsorption properties of the three molecules exhibit significant changes due to the spatial confinement within the microenvironment. The original spacing of 3.20 Å between graphene and the Pd(111) substrate cannot completely accommodate the molecules. Thus, upon their intercalation, the vertical position and the morphology of the graphene overlayer change substantially. On the one hand, graphene needs to be moved away from the substrate to provide more space for the intercalating molecules; while on the other hand, the bonding of graphene with the substrate attempts to keep it at its original height. The competition of these two factors brings about the deformation of graphene as shown in the right panel of Figure 3. One can see that the carbon atoms of graphene that are directly above the molecules move far away from the substrate, while other carbon atoms show relatively small displacements. The deformation of graphene destabilizes the interface system and thereby result in a decrease in the adsorption strength of the molecules. Here, the adsorption energies of C_2H_2, C_2H_4, and C_2H_6 change from −2.53, −1.43, and −0.40 eV to −1.32, +0.55, and +3.65 eV, respectively, corresponding to weakening by 1.21, 1.98, and 4.05 eV. Moreover, the average distance between carbon atoms of graphene and the Pd(111) substrate increases to 3.55, 3.66, and 5.04 Å, and the undulation of the graphene overlayer, i.e., the maximum difference in the vertical coordinates of the carbon atoms, becomes 1.08, 1.27, and 0.97 Å, respectively. From a thermodynamic point of view, only C_2H_2 can be intercalated into the sub-nanocontainer, while C_2H_4 and C_2H_6 will be repelled by the microenvironment. It indicates that once the acetylene molecules participate in the hydrogenation reactions within the sub-nanocontainer, the hydrogenation process could stop at the stage of ethylene production and will not move forward in the microenvironment.

3.3. Energy Profiles of the Hydrogenation Reactions on Pd(111) and Within the Pd(111)/Graphene Sub-Nanospace. The energy profiles of the hydrogenation reactions on the Pd(111) surface (blue lines) and within the Pd(111)/graphene interface (red lines) are presented in Figure 4. The whole process starts with the adsorption of C_2H_2 and

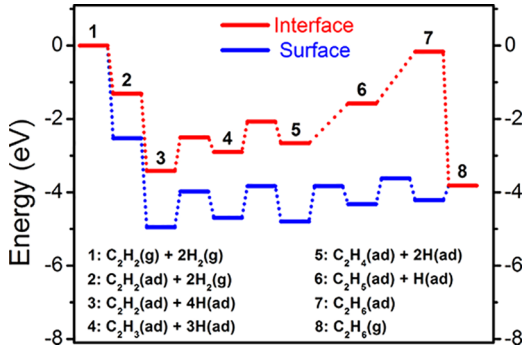

Figure 4. Calculated energy diagrams for the hydrogenation of acetylene to ethane on the Pd(111) surface (blue) and within the Pd(111)/graphene interface (red).

H_2, ends with C_2H_6 desorption, and includes four successive hydrogenation steps in between. Here, the formation pathway of hydrocarbons that are larger than methane was not considered. It is because, within the microenvironment, the formation of larger hydrocarbons will be inhibited to a greater extent than that of methane. Compared with methane, larger molecules make the 2D monolayer be further away from the Pd substrate and exhibit more severe deformation. As is shown in Figure 4, there is a significant overall difference between the two energy diagrams in the last two hydrogenation steps, i.e., $C_2H_4 + H \rightarrow C_2H_5$ (5 → 6) and $C_2H_5 + H \rightarrow C_2H_6$ (6 → 7). The reaction energies of the two steps are 0.48 and 0.11 eV on the Pd(111) surface but increase to 1.08 and 1.41 eV for the Pd(111)/graphene interface. Such a contrast demonstrates that from a thermodynamic point of view, the formation of ethane via overhydrogenation of ethylene becomes much more difficult upon coverage with the graphene overlayer. Moreover, since the two steps within the microenvironment are continuously endothermic, the kinetic energy barrier should be the sum of the two reaction energies, that is, 2.49 eV, which is much higher than that of 1.18 eV on bare Pd(111). Such a high energy barrier means that with the involvement of graphene, the overhydrogenation toward ethane is significantly inhibited. Regarding the first two hydrogenation steps, the reaction energies (0.52 and 0.24 eV) that are obtained inside the sub-nanospace are slightly larger than the values (0.26 and −0.10 eV) on the Pd(111) surface, and the corresponding energy barrier of 1.34 eV within the microenvironment is just a bit higher than that of 1.12 eV on Pd(111). The above results indicate that placing C_2H_2 reactants in the microenvironment can effectively hinder the unwanted overhydrogenation process toward C_2H_6. Thus, with the involvement of the graphene overlayer, a significant improvement in the selectivity of acetylene hydrogenation could be achieved. It may be worth mentioning that although the acetylene reactant is energetically more favorable on the bare Pd surface than within the confined sub-nanospace, a large portion of the reactant can still be hydrogenated in the microenvironment if most of the Pd

https://dx.doi.org/10.1021/acsami.0c12437
ACS Appl. Mater. Interfaces 2020, 12, 39352−39361

surface is covered by graphene. We note that the enhanced selectivity of acetylene hydrogenation has indeed be verified in experiments using encapsulated PdZn nanoparticles as catalysts.[56]

3.4. Intercalation of C_2H_2 into the Pd(111)/Graphene Sub-Nanospace on Pd(111). With the confirmation of improved selectivity in the hydrogenation reactions, we now move to the next question—how the C_2H_2 molecules intercalate into the sub-nanospace. Previous experimental studies have suggested that the intercalated molecules can enter the microenvironment via inlets of graphene edges[57,58] or defects.[58] Here, considering that acetylene has a linear geometry, its most likely approach of entering the sub-nanospace may be drilling into the regions below graphene edges, as had been adopted in previous simulations.[59,60] Among the three types of edge configurations of graphene (zigzag, armchair, and chiral), the zigzag type is considered in our investigation since the serrated pattern of the edge carbon atoms could be able to reduce the steric repulsions for linear molecules like acetylene and thereby make their entry easier than the situations of the other two types. It is also worth noting that the edge carbon atoms of graphene are saturated by hydrogen atoms, as the whole system is placed in a H_2 atmosphere during the hydrogenation reactions. Despite that, the carbon atoms at the edge of graphene may not be fully (100%) saturated with hydrogen atoms, and thus, a very small proportion (5.6%) of hydrogen atoms is missing in the model. The corresponding simulation model is shown in Figure S3.

In Figure 5, we present a few selected intermediate states in the entire process of a C_2H_2 molecule entering the sub-nanospace. The corresponding adsorption energies are given in the lower right corners of the respective figures. We propose that the diffusion of acetylene on Pd(111) occurs along the direction of its carbon−carbon triple bond, which is perpendicular to the zigzag edge of the graphene overlayer (Figure 5A−C). As the acetylene molecule arrives at the area that is directly below the edge region, it could change its adsorption structure back and forth via small-angle rotations between the μ-bridge (Figure 5E) and the ‖-bridge (Figure 5D,F) configurations, and in this way, it enters the sub-nanospace. After that, the acetylene molecule could continue to diffuse within the microenvironment and be steered by the undulation of the graphene overlayer (Figure 5G,H). The existence of the hydrogen vacancies provides effective channels for acetylene intercalation. The diagram in Figure 5 reveals two things: First, since the adsorption energies are all negative, the occurrence of the above diffusion is allowable from a thermodynamic point of view. Second, due to the endothermic characteristic of the acetylene insertion and the rather low diffusion barriers of C_2H_2 on bare Pd(111),[52] the intercalation process (Figure 5A−F) seems to be thermodynamically determined. In other words, the energy barriers are expected to be equal to the reaction energies of the corresponding endothermic processes, reminiscent of the two overhydrogenation steps from ethylene to ethane in the sub-nanospace (red line in Figure 4) where no transition state is involved. It is worth noting that curved geometries such as wrinkles of graphene or atomic steps of the substrate may exist at the Pd(111)/graphene interface as in the case of Ir(111)/graphene.[61] Moreover, at the reaction temperature, the acetylene molecules may become more flexible and the inlet may also exhibit breathing motions. All of the above factors could further reduce the obstacles for acetylene intercalation.

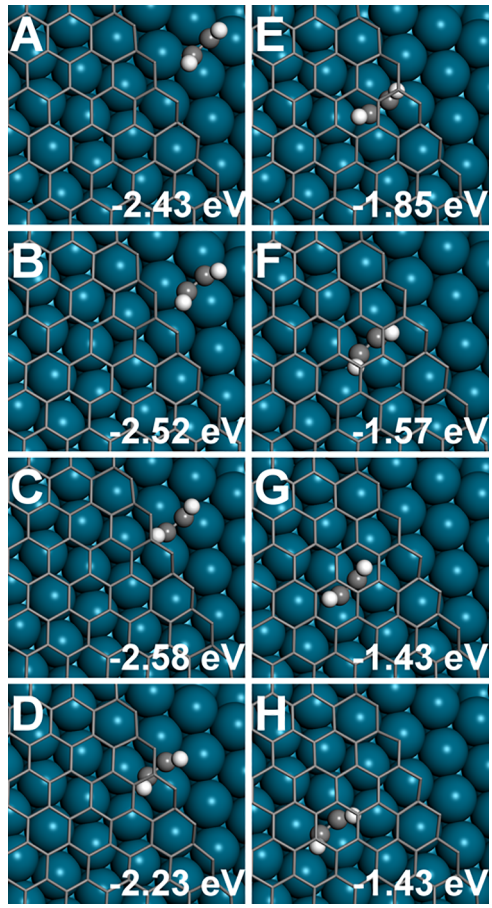

Figure 5. Selected intermediate states (A−H) in the entire process of a C_2H_2 molecule entering the sub-nanospace formed by graphene and Pd(111). The adsorption energies of C_2H_2 are labeled in the lower right corners of the respective figures. The hydrogen atoms that are used to saturate the edge carbon atoms are not shown for the sake of clarity.

Due to the huge complexity regarding this process, however, a comprehensive investigation of all involved elementary steps is beyond the scope of this work and thus was not performed.

Experimentally, the intercalation of CO into the sub-nanospace was shown to occur easily when its partial pressure was raised to 1×10^{-6} mbar.[58] Compared to this case, the intercalation of C_2H_2 is expected to be even easier. It is because, on a transition-metal surface, CO exhibits a vertical adsorption configuration in which the distance between the outermost layer of the transition-metal substrate and the O atom in CO is 3.0 Å.[34] For the adsorption of C_2H_2, the molecule adopts a parallel configuration on the substrate, and the distance between the outermost metal layer and the H atoms is reduced to 2.4 Å. Since the intercalation process of the molecules unavoidably involves an increase in the distance between the graphene edges and the transition-metal surface, the edge carbon atoms bend upward to a lesser extent in the insertion of C_2H_2 than that of CO, corresponding to a smaller energy barrier in the former case. This comparison has been well demonstrated in our simulations. From Figures 5 and S4, one can see that the energy barrier of CO entry (1.76 eV) is much higher than that of C_2H_2 insertion (1.00 eV). Thus, the entry of C_2H_2 into the microenvironment can occur, and the threshold of the partial pressure for the intercalation is expected to be less than that of carbon monoxide, that is, $1 \times$

https://dx.doi.org/10.1021/acsami.0c12437
ACS Appl. Mater. Interfaces 2020, 12, 39352−39361

10^{-6} mbar, which corresponds to a concentration of less than 0.001 ppm when the pressure of ethylene gas is 1 atm. The value of 0.001 ppm is much lower than the actual acetylene concentration of 1% in the industrially produced ethylene feedstock, meaning that under the actual reaction conditions, the acetylene molecules could be able to enter the sub-nanospace to participate in the hydrogenation reactions. As another participant in the hydrogenation reaction, hydrogen atoms also need to enter the sub-nanoreactor. Since a hydrogen atom is much smaller than an acetylene molecule, the entry of the former is much easier than that of the latter. As a result, the acetylene molecules within the sub-nanoreactor will be located in a highly hydrogen-rich environment, which can effectively suppress the formation of coke.

3.5. Effects of Adsorbate Coverage on the Adsorption and Reaction Properties. It is known that once the coverage of adsorbed molecules on a substrate is altered, for example, by varying temperature or partial pressure, adsorption and reaction properties of the adsorbates could be changed accordingly. We thus explore a situation at a higher C_2H_x (x = 2, 4, and 6) coverage. To this extent, the coverage of the adsorbates is increased by a factor of 4, that is, one adsorbed molecule corresponds to seven Pd atoms in the surface layer. We find that the most stable configurations of C_2H_2, C_2H_4, and C_2H_6 on Pd(111) do not change, with the corresponding adsorption energies being −2.49, −1.40, and −0.41 eV, respectively, very close to the values (−2.53, −1.43, and −0.40 eV) at the original coverage. It means that, on the bare Pd(111) surface, a change in the coverage does not make a big difference in the adsorption behavior of the molecules. In the sub-nanospace of the Pd(111)/graphene interface, by contrast, the properties become very different. With the coverage of the adsorbates being increased, the graphene overlayer becomes significantly away from the substrate and maintains its planar structure as shown in Figure 6. The distances between

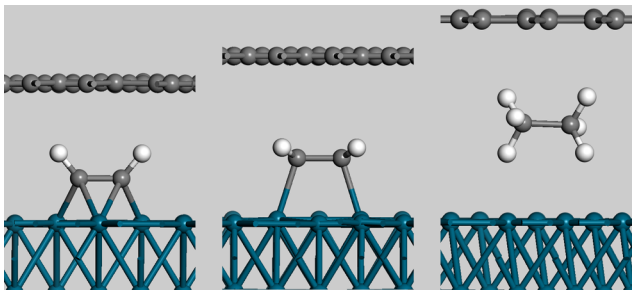

Figure 6. Adsorption structures of C_2H_2 (left), C_2H_4 (middle), and C_2H_6 (right) molecules within the sub-nanospace between Pd(111) and the graphene overlayer. The results are obtained at the coverage of adsorbates increased by a factor of 4.

graphene and the outermost layer of Pd(111) increases to 4.62, 5.47, and 6.41 Å, respectively. The adsorption energies of the three molecules are calculated to be −1.72, −0.51, and +0.65 eV, corresponding to weakening of the adsorption by 0.77, 0.88, and 1.06 eV, respectively. Here, compared to the weakening at the original lower coverage (being 1.21, 1.98, and 4.05 eV, respectively), the corresponding extents are significantly reduced, especially for that of ethane. This phenomenon comes from the fact that as the coverage increases, the number of the adsorbates under the same area of graphene becomes larger, and therefore, the energy penalty due to the lifting of the graphene overlayer is borne by more adsorbates. Nevertheless, it should be mentioned that although the adsorption properties within the microenvironment vary greatly with coverage, the adsorption of ethane is still energetically unfavorable, meaning that even at large coverage, the overhydrogenation of acetylene can still be thermodynamically inhibited.

In Figure 7, we present the calculated energy diagrams of the hydrogenation reactions at the increased coverage of

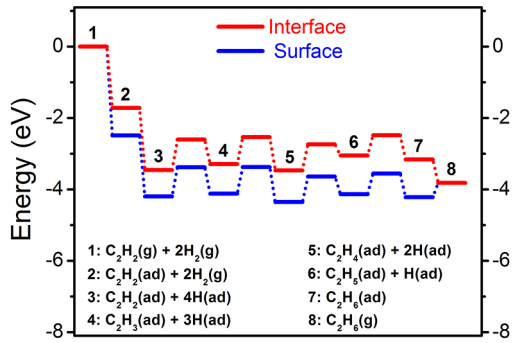

Figure 7. Calculated energy diagrams for the hydrogenation of acetylene toward ethane on the Pd(111) surface (blue) and within the Pd(111)/graphene interface (red). The results are obtained at the coverage of adsorbates increased by a factor of 4.

adsorbates on both the Pd(111) surface (blue line) and within the Pd(111)/graphene interface (red line). Although the difference in the characteristics of the diagram between the surface and the interface is not as obvious as that in Figure 4, the presence of graphene still plays a role in improving the selectivity of the hydrogenation reaction. On the Pd(111) surface, the total energy barrier of the two overhydrogenation reaction steps ($C_2H_4 + 2H \rightarrow C_2H_6$) is calculated to be 0.80 eV, which is slightly smaller than the corresponding barrier of 0.83 eV in the first two steps. It means that once ethylene is formed on the bare Pd(111) surface, its further hydrogenation toward ethane is even easier than the hydrogenation of acetylene. Within the subnano space, by contrast, the energy barrier in the overhydrogenation steps (0.98 eV) becomes larger than that in ethylene production (0.92 eV). These results indicate that in the case of high coverage, placing graphene on Pd(111) could still be able to inhibit the formation of ethane, which, accordingly, helps in increasing the selectivity toward the desired ethylene products.

3.6. Adsorption and Reaction Inside the Pd(111)/h-BN Sub-Nanospace. Besides graphene, other 2D materials can also be deposited on transition-metal surfaces. Due to the differences in the geometry and the interaction with the substrates, altering 2D materials that cover Pd(111) may affect the hydrogenation process inside the produced microenvironment. Here, we use h-BN as an example to investigate such an effect. Previous experiments showed that covering h-BN on Pt(111) can effectively weaken CO adsorption and enhance the CO oxidation reaction.[62,63] Although h-BN has the same atomic arrangement as graphene, its lattice constant is larger than the latter (2.511 Å vs 2.467 Å), and thus, the h-BN overlayer undergoes greater compressive stress (3.04% vs 1.28% of graphene) when forming an interface with Pd(111). In fact, a slight difference of 0.044 Å in the lattice constant causes significant changes in the morphology of the interface. As shown in Figure 8, the h-BN monolayer that covers

https://dx.doi.org/10.1021/acsami.0c12437
ACS Appl. Mater. Interfaces 2020, 12, 39352−39361

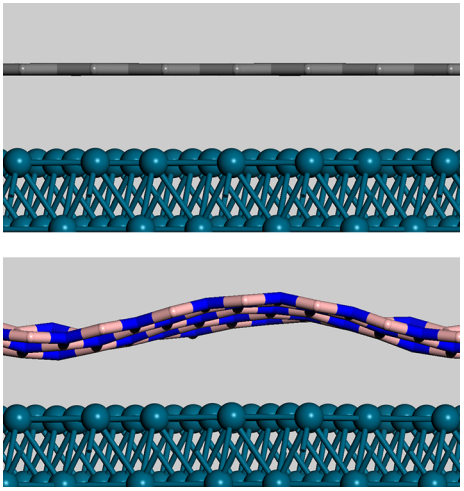

Figure 8. Configurations of Pd(111)/graphene (top) and Pd(111)/h-BN (bottom) interfaces. The Pd, B, C, and N atoms are depicted in teal blue, pink, gray, and blue, respectively.

Pd(111) exhibits dramatic undulation (bottom panel), in sharp contrast to the planar structure of the graphene overlayer (top panel). The binding energy of the two components and the average distance between h-BN and the outermost layer of Pd(111) are calculated to be −5.65 eV and 3.19 Å, respectively, very close to the values of −5.80 eV and 3.19 Å in the case of graphene. The presence of intrinsic undulation indicates that once the molecules are intercalated into the sub-nanospace, the penalty in the adsorption energies caused by the deformation of the 2D overlayer will be smaller in the case of h-BN compared to that of graphene. As expected, the calculated adsorption energies of acetylene, ethylene, and ethane within the Pd(111)/h-BN microenvironment are −2.19, −0.65, and +1.72 eV, respectively, corresponding to the adsorption weakening by 0.34, 0.77, and 2.12 eV under the h-BN overlayer. These three values are remarkably smaller than the adsorption energy changes of 1.21, 1.98, and 4.05 eV in the case of the Pd(111)/graphene interface. This demonstrates that the curvature of the 2D monolayer over the transition-metal surface is one factor of affecting the variation of the adsorption energies. Moreover, within the sub-nanospace, the adsorption of ethane is also energetically unfavorable, which means that, thermodynamically, the undesired overhydrogenation of acetylene can still be effectively inhibited.

In Figure 9, we present the calculated energy diagram for the hydrogenation of acetylene within the Pd(111)/h-BN interface (red line). For comparison, the corresponding diagram on the bare Pd(111) surface is also shown (blue line). One can see that upon covering by h-BN, the total energy barrier of the reaction $C_2H_4 + 2H \rightarrow C_2H_6$ increases from 1.18 eV on bare Pd(111) to 1.79 eV inside the microenvironment, again demonstrating that the unwanted overhydrogenation toward ethane can be remarkably hindered. It is also interesting to find that in the first two steps, i.e., $C_2H_2 + 2H \rightarrow C_2H_4$, the energy barrier within the sub-nanospace is even 0.10 eV lower than that on the Pd(111) surface (1.02 eV vs 1.12 eV). This means that with the involvement of h-BN, the hydrogenation process from acetylene to ethylene becomes easier. The above results indicate that the h-BN monolayer could be superior to graphene in improving the catalytic performance of the underlying transition-metal substrates. It also indicates that a slight adjustment on the stress of the overlayer could lead to

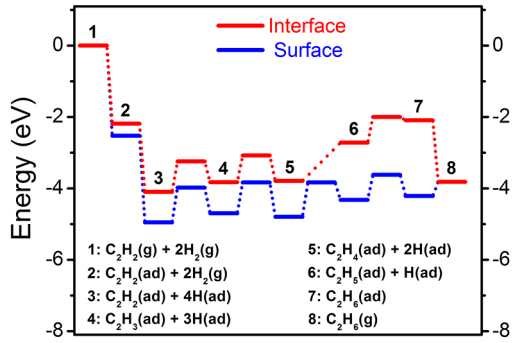

Figure 9. Calculated energy diagrams for the hydrogenation of acetylene toward ethane on the Pd(111) surface (blue line) and within the Pd(111)/h-BN interface (red line). The original coverage of adsorbates (one molecule corresponds to 28 Pd surface atoms) is adopted.

significant changes in the reaction properties within the microenvironment.

3.7. Covering Graphene on the Pd-Doped Ag(111) Substrate. Since monometallic Pd catalysts suffer from low selectivity in catalyzing the hydrogenation reaction from acetylene to ethylene, bimetallic Pd−Ag alloy systems are commonly employed in industry.[64,65] Adding Ag to Pd not only increases the selectivity of the reaction but also promotes the catalyst's lifetime by, e.g., inhibiting green oil formation and coke deposition.[11,66,67] Moreover, considering that the price of Ag is only one percent of that of Pd, replacing part of the Pd atoms with Ag atoms can reduce the cost of the catalyst. The ultimate pattern of replacing Pd in the Ag−Pd bimetallic systems is to form Pd single-atom alloys,[68,69] where a very low concentration of isolated single Pd atoms is embedded in the Ag hosting substrate. Previous experiments showed that the Pd single-atom catalyst (SAC) hosted by Ag exhibits excellent acetylene conversion and selectivity toward ethylene.[10] It is thus natural to ask whether the selectivity of acetylene hydrogenation can be further improved by forming a sub-nanospace between graphene and the Pd SAC.

In the Pd SAC model, the doping concentration of Pd at the Ag(111) surface layer is 4.2% and one C_2H_x (x = 2, 4, and 6) molecule corresponds to 24 metal atoms. Upon formation of the SAC/graphene interface, the distance between the two components is 3.41 Å, 0.22 Å larger than the corresponding distances for the Pd(111)/graphene and Pd(111)/h-BN interfaces. This larger spatial spacing indicates that the interaction between the SAC surface and the graphene overlayer is weaker than those in Pd(111)/graphene and Pd(111)/h-BN, which is further verified by the calculated binding energies. Our results show that the interaction in the former is weaker by more than 1 eV than those in the latter two systems (converted to the same interface area), which originates from the lower reactivity of Ag(111) than that of Pd(111). The decrease in the reactivity causes significant changes in the adsorption energies of acetylene, ethylene, and ethane. On the SAC surface, the three adsorption energies are calculated to be −0.82, −0.86, and −0.33 eV, respectively, which are remarkably reduced compared with the values on Pd(111). Here, the three adsorption energies are too small to compensate the energy penalties for lifting and deforming the graphene overlayer, which makes the intercalation of all the three molecules energetically unfavorable within the sub-nanospace. The adsorption energies in the microenvironment

https://dx.doi.org/10.1021/acsami.0c12437
ACS Appl. Mater. Interfaces 2020, 12, 39352−39361

are calculated to be +0.45, +0.89, and +2.95 eV, respectively, meaning that all the molecules cannot enter the region between graphene and SAC. This demonstrates that the strength of the interactions between adsorbates and transition-metal substrates is another factor of affecting the adsorption energies within the microenvironment. These results suggest that the strategies of spatial confinement and single-atom catalysis could not be combined to improve the selectivity of acetylene hydrogenation. To address this issue, a more reactive hosting surface than Ag would be required to accommodate isolated single Pd atoms.

4. CONCLUSIONS

To conclude, by performing first-principles calculations, we have shown that one can improve the selectivity of hydrogenation reactions by means of spatial confinement exerted by the sub-nanospace between two-dimensional (2D) monolayers and transition-metal substrates. The presence of graphene or a hexagonal boron nitride monolayer can affect the adsorption energies of acetylene, ethylene, and ethane inside the sub-nanospace to varying extents, thereby changing the energy profile of the entire hydrogenation progress. As such, the overhydrogenation toward ethane can be significantly inhibited. Changes in the coverage of adsorbates and the strain within 2D monolayers can affect the influence of the spatial confinement on the adsorption properties, which may have important implications in tuning the catalytic performance of the sub-nanospace. We have also taken the sub-nanospace between graphene and a Pd-doped Ag(111) substrate as an example to show that the strategies of spatial confinement and single-atom catalysis could not be combined for improving hydrogenation selectivity. With these findings, we highlight the belief that "*there is plenty of room*" inside the sub-nanospace and propose a new strategy of designing novel catalysts for the selective hydrogenation of acetylene.

■ ASSOCIATED CONTENT

Supporting Information

The Supporting Information is available free of charge at https://pubs.acs.org/doi/10.1021/acsami.0c12437.

Display of the lattices for Ag(111) and graphene in the interface model construction; density of states (DOS) of the *d* electrons of Pd(111) before and after the coverage of graphene; simulation model of the inlet region for acetylene intercalation; selected intermediate states in the entire process of a CO molecule entering the sub-nanospace formed by graphene and Pd(111) (PDF)

■ AUTHOR INFORMATION

Corresponding Author

Qiang Fu − *School of Chemistry and Chemical Engineering, Shandong University, Jinan 250100, China; Institut für Physik and IRIS Adlershof, Humboldt-Universität zu Berlin, Berlin 12489, Germany;* orcid.org/0000-0002-6682-8527; Email: qfu@sdu.edu.cn

Authors

Fan Wu − *School of Chemistry and Chemical Engineering, Shandong University, Jinan 250100, China*

Bingxue Wang − *School of Chemistry and Chemical Engineering, Shandong University, Jinan 250100, China*

Yuxiang Bu − *School of Chemistry and Chemical Engineering, Shandong University, Jinan 250100, China;* orcid.org/0000-0002-6445-5069

Claudia Draxl − *Institut für Physik and IRIS Adlershof, Humboldt-Universität zu Berlin, Berlin 12489, Germany; Fritz-Haber-Institut der Max-Planck-Gesellschaft, Berlin 14195, Germany;* orcid.org/0000-0003-3523-6657

Complete contact information is available at: https://pubs.acs.org/10.1021/acsami.0c12437

Notes

The authors declare no competing financial interest.

■ ACKNOWLEDGMENTS

Q.F. is grateful for the funding from the National Natural Science Foundation of China (21803036), the Shandong Provincial Natural Science Foundation, China (ZR2018QB005), the Young Scholars Program of Shandong University (2018WLJH49), and the Taishan Scholars Project of Shandong Province (ts201712011). Q.F. and C.D. appreciate support from the European Union's Horizon 2020 research and innovation programme, Grant Agreement No. 676580 through the Center of Excellence NOMAD (Novel Materials Discovery Laboratory, https://NOMAD-CoE.eu). First-principles calculations were performed on the HPC Cloud Platform of Shandong University and the high-performance computing cluster DUNE at Humboldt-Universität zu Berlin.

■ REFERENCES

(1) Tunuguntla, R. H.; Henley, R. Y.; Yao, Y.-C.; Pham, T. A.; Wanunu, M.; Noy, A. Enhanced Water Permeability and Tunable Ion Selectivity in Subnanometer Carbon Nanotube Porins. *Science* **2017**, *357*, 792−796.

(2) Küchler, A.; Yoshimoto, M.; Luginbühl, S.; Mavelli, F.; Walde, P. Enzymatic Reactions in Confined Environments. *Nat. Nanotechnol.* **2016**, *11*, 409−420.

(3) Pan, X.; Fan, Z.; Chen, W.; Ding, Y.; Luo, H.; Bao, X. Enhanced Ethanol Production inside Carbon-Nanotube Reactors Containing Catalytic Particles. *Nat. Mater.* **2007**, *6*, 507−511.

(4) Xiao, J.; Pan, X.; Guo, S.; Ren, P.; Bao, X. Toward Fundamentals of Confined Catalysis in Carbon Nanotubes. *J. Am. Chem. Soc.* **2015**, *137*, 477−482.

(5) Dong, B.; Pei, Y.; Zhao, F.; Goh, T. W.; Qi, Z.; Xiao, C.; Chen, K.; Huang, W.; Fang, N. In situ Quantitative Single-Molecule Study of Dynamic Catalytic Processes in Nanoconfinement. *Nat. Catal.* **2018**, *1*, 135−140.

(6) Zhao, H.; Sen, S.; Udayabhaskararao, T.; Sawczyk, M.; Kucanda, K.; Manna, D.; Kundu, P. K.; Lee, J. W.; Král, P.; Klajn, R. Reversible Trapping and Reaction Acceleration within Dynamically Self-Assembling Nanoflasks. *Nat. Nanotechnol.* **2016**, *11*, 82−88.

(7) Petrosko, S. H.; Johnson, R.; White, H.; Mirkin, C. A. Nanoreactors: Small Spaces, Big Implications in Chemistry. *J. Am. Chem. Soc.* **2016**, *138*, 7443−7445.

(8) Hecht, S. Chemistry in and out of Nanoflasks. *Nat. Nanotechnol.* **2016**, *11*, 6−7.

(9) McCue, A. J.; Anderson, J. A. Recent Advances in Selective Acetylene Hydrogenation Using Palladium Containing Catalysts. *Front. Chem. Sci. Eng.* **2015**, *9*, 142−153.

(10) Pei, G. X.; Liu, X. Y.; Wang, A.; Lee, A. F.; Isaacs, M. A.; Li, L.; Pan, X.; Yang, X.; Wang, X.; Tai, Z.; Wilson, K.; Zhang, T. Ag Alloyed Pd Single-Atom Catalysts for Efficient Selective Hydrogenation of Acetylene to Ethylene in Excess Ethylene. *ACS Catal.* **2015**, *5*, 3717−3725.

(11) Liu, D. DFT Study of Selective Hydrogenation of Acetylene to Ethylene on Pd Doping Ag Nanoclusters. *Appl. Surf. Sci.* **2016**, *386*, 125−137.
(12) Feng, Q.; et al. Isolated Single-Atom Pd Sites in Intermetallic Nanostructures: High Catalytic Selectivity for Semihydrogenation of Alkynes. *J. Am. Chem. Soc.* **2017**, *139*, 7294−7301.
(13) Xu, L.; Stangland, E. E.; Mavrikakis, M. Ethylene versus Ethane: A DFT-based Selectivity Descriptor for Efficient Catalyst Screening. *J. Catal.* **2018**, *362*, 18−24.
(14) Studt, F.; Abild-Pedersen, F.; Bligaard, T.; Sorensen, R. Z.; Christensen, C. H.; Norskov, J. K. Identification of Non-Precious Metal Alloy Catalysts for Selective Hydrogenation of Acetylene. *Science* **2008**, *320*, 1320−1322.
(15) Pei, G. X.; Liu, X. Y.; Wang, A.; Su, Y.; Li, L.; Zhang, T. Selective Hydrogenation of Acetylene in an Ethylene-Rich Stream over Silica Supported Ag-Ni Bimetallic Catalysts. *Appl. Catal., A* **2017**, *545*, 90−96.
(16) Ahn, I. Y.; Lee, J. H.; Kim, S. K.; Moon, S. H. Three-Stage Deactivation of Pd/SiO_2 and $Pd-Ag/SiO_2$ Catalysts during the Selective Hydrogenation of Acetylene. *Appl. Catal., A* **2009**, *360*, 38−42.
(17) Pachulski, A.; Schödel, R.; Claus, P. Performance and Regeneration Studies of $Pd-Ag/Al_2O_3$ Catalysts for the Selective Hydrogenation of Acetylene. *Appl. Catal., A* **2011**, *400*, 14−24.
(18) Tao, F.; Grass, M. E.; Zhang, Y.; Butcher, D. R.; Renzas, J. R.; Liu, Z.; Chung, J. Y.; Mun, B. S.; Salmeron, M.; Somorjai, G. A. Reaction-Driven Restructuring of Rh−Pd and Pt−Pd Core-Shell Nanoparticles. *Science* **2008**, *322*, 932−934.
(19) Cui, C.; Gan, L.; Heggen, M.; Rudi, S.; Strasser, P. Compositional Segregation in Shaped Pt Alloy Nanoparticles and Their Structural Behaviour during Electrocatalysis. *Nat. Mater.* **2013**, *12*, 765−771.
(20) Vignola, E.; Steinmann, S. N.; Al Farra, A.; Vandegehuchte, B. D.; Curulla, D.; Sautet, P. Evaluating the Risk of C−C Bond Formation during Selective Hydrogenation of Acetylene on Palladium. *ACS Catal.* **2018**, *8*, 1662−1671.
(21) Huang, F.; Deng, Y.; Chen, Y.; Cai, X.; Peng, M.; Jia, Z.; Ren, P.; Xiao, D.; Wen, X.; Wang, N.; Liu, H.; Ma, D. Atomically Dispersed Pd on Nanodiamond/Graphene Hybrid for Selective Hydrogenation of Acetylene. *J. Am. Chem. Soc.* **2018**, *140*, 13142−13146.
(22) Nørskov, J. K.; Bligaard, T.; Hvolbæk, B.; Abild-Pedersen, F.; Chorkendorff, I.; Christensen, C. H. The Nature of the Active Site in Heterogeneous Metal Catalysis. *Chem. Soc. Rev.* **2008**, *37*, 2163.
(23) Andersen, M.; Medford, A. J.; Nørskov, J. K.; Reuter, K. Analyzing the Case for Bifunctional Catalysis. *Angew. Chem., Int. Ed.* **2016**, *55*, 5210−5214.
(24) Andersen, M.; Medford, A. J.; Nørskov, J. K.; Reuter, K. Scaling-Relation-Based Analysis of Bifunctional Catalysis: The Case for Homogeneous Bimetallic Alloys. *ACS Catal.* **2017**, *7*, 3960−3967.
(25) Kumar, G.; Nikolla, E.; Linic, S.; Medlin, J. W.; Janik, M. J. Multicomponent Catalysts: Limitations and Prospects. *ACS Catal.* **2018**, *8*, 3202−3208.
(26) Marshall, S. T.; O'Brien, M.; Oetter, B.; Corpuz, A.; Richards, R. M.; Schwartz, D. K.; Medlin, J. W. Controlled Selectivity for Palladium Catalysts Using Self-Assembled Monolayers. *Nat. Mater.* **2010**, *9*, 853−858.
(27) Kahsar, K. R.; Schwartz, D. K.; Medlin, J. W. Control of Metal Catalyst Selectivity through Specific Noncovalent Molecular Interactions. *J. Am. Chem. Soc.* **2014**, *136*, 520−526.
(28) Schrader, I.; Warneke, J.; Backenköhler, J.; Kunz, S. Functionalization of Platinum Nanoparticles with L-Proline: Simultaneous Enhancements of Catalytic Activity and Selectivity. *J. Am. Chem. Soc.* **2015**, *137*, 905−912.
(29) Dostert, K. H.; O'Brien, C. P.; Ivars-Barceló, F.; Schauermann, S.; Freund, H. J. Spectators Control Selectivity in Surface Chemistry: Acrolein Partial Hydrogenation over Pd. *J. Am. Chem. Soc.* **2015**, *137*, 13496−13502.
(30) Wang, Y.; Wan, X. K.; Ren, L.; Su, H.; Li, G.; Malola, S.; Lin, S.; Tang, Z.; Häkkinen, H.; Teo, B. K.; Wang, Q. M.; Zheng, N. Atomically Precise Alkynyl-Protected Metal Nanoclusters as a Model Catalyst: Observation of Promoting Effect of Surface Ligands on Catalysis by Metal Nanoparticles. *J. Am. Chem. Soc.* **2016**, *138*, 3278−3281.
(31) Chen, T.; Rodionov, V. O. Controllable Catalysis with Nanoparticles: Bimetallic Alloy Systems and Surface Adsorbates. *ACS Catal.* **2016**, *6*, 4025−4033.
(32) Zhao, X.; Zhou, L.; Zhang, W.; Hu, C.; Dai, L.; Ren, L.; Wu, B.; Fu, G.; Zheng, N. Thiol Treatment Creates Selective Palladium Catalysts for Semihydrogenation of Internal Alkynes. *Chem* **2018**, *4*, 1080−1091.
(33) Yao, Y.; Fu, Q.; Zhang, Y. Y.; Weng, X.; Li, H.; Chen, M.; Jin, L.; Dong, A.; Mu, R.; Jiang, P.; Liu, L.; Bluhm, H.; Liu, Z.; Zhang, S. B.; Bao, X. Graphene Cover-Promoted Metal-Catalyzed Reactions. *Proc. Natl. Acad. Sci. U.S.A.* **2014**, *111*, 17023−17028.
(34) Li, H.; Xiao, J.; Fu, Q.; Bao, X. Confined Catalysis under Two-Dimensional Materials. *Proc. Natl. Acad. Sci. U.S.A.* **2017**, *114*, 5930−5934.
(35) Fu, Q.; Bao, X. Surface Chemistry and Catalysis Confined under Two-Dimensional Materials. *Chem. Soc. Rev.* **2017**, *46*, 1842−1874.
(36) Chung, D. Y.; et al. Highly Durable and Active PtFe Nanocatalyst for Electrochemical Oxygen Reduction Reaction. *J. Am. Chem. Soc.* **2015**, *137*, 15478−15485.
(37) Gao, L.; Fu, Q.; Li, J.; Qu, Z.; Bao, X. Enhanced CO Oxidation Reaction over Pt Nanoparticles Covered with Ultrathin Graphitic Layers. *Carbon* **2016**, *101*, 324−330.
(38) Zhou, Y.; Chen, W.; Cui, P.; Zeng, J.; Lin, Z.; Kaxiras, E.; Zhang, Z. Enhancing the Hydrogen Activation Reactivity of Nonprecious Metal Substrates via Confined Catalysis Underneath Graphene. *Nano Lett.* **2016**, *16*, 6058−6063.
(39) Li, B.; Nam, H.; Zhao, J.; Chang, J.; Lingappan, N.; Yao, F.; Lee, T. H.; Lee, Y. H. Nanoreactor of Nickel-Containing Carbon-Shells as Oxygen Reduction Catalyst. *Adv. Mater.* **2017**, *29*, No. 1605083.
(40) Gao, L.; Wang, Y.; Li, H.; Li, Q.; Ta, N.; Zhuang, L.; Fu, Q.; Bao, X. A Nickel Nanocatalyst within a h-BN Shell for Enhanced Hydrogen Oxidation Reactions. *Chem. Sci.* **2017**, *8*, 5728−5734.
(41) Zhang, L.; Ding, Y.; Wu, K.-H.; Niu, Y.; Luo, J.; Yang, X.; Zhang, B.; Su, D. Pd@C Core-Shell Nanoparticles on Carbon Nanotubes as Highly Stable and Selective Catalysts for Hydrogenation of Acetylene to Ethylene. *Nanoscale* **2017**, *9*, 14317−14321.
(42) Fu, Q.; Rausseo, L. C. C.; Martinez, U.; Dahl, P. I.; Lastra, J. M. G.; Vullum, P. E.; Svenum, I.-H.; Vegge, T. Effect of Sb Segregation on Conductance and Catalytic Activity at Pt/Sb-Doped SnO_2 Interface: A Synergetic Computational and Experimental Study. *ACS Appl. Mater. Interfaces* **2015**, *7*, 27782−27795.
(43) Kresse, G.; Furthmüller, J. Efficiency of Ab-Initio Total Energy Calculations for Metals and Semiconductors Using a Plane-Wave Basis Set. *Comput. Mater. Sci.* **1996**, *6*, 15−50.
(44) Kresse, G.; Furthmüller, J. Efficient Iterative Schemes for Ab Initio Total-Energy Calculations Using a Plane-Wave Basis Set. *Phys. Rev. B* **1996**, *54*, No. 11169.
(45) Blöchl, P. E. Projector Augmented-Wave Method. *Phys. Rev. B* **1994**, *50*, No. 17953.
(46) Dion, M.; Rydberg, H.; Schröder, E.; Langreth, D. C.; Lundqvist, B. I. Van der Waals Density Functional for General Geometries. *Phys. Rev. Lett.* **2004**, *92*, No. 246401.
(47) Klimeš, J.; Bowler, D. R.; Michaelides, A. Chemical Accuracy for the Van der Waals Density Functional. *J. Phys.: Condens. Matter* **2010**, *22*, No. 022201.
(48) Klimeš, J.; Bowler, D. R.; Michaelides, A. Van der Waals Density Functionals Applied to Solids. *Phys. Rev. B* **2011**, *83*, No. 195131.
(49) Monkhorst, H. J.; Pack, J. D. Special Points for Brillouin-Zone Integrations. *Phys. Rev. B* **1976**, *13*, No. 5188.
(50) Henkelman, G.; Uberuaga, B. P.; Jónsson, H. A Climbing Image Nudged Elastic Band Method for Finding Saddle Points and Minimum Energy Paths. *J. Chem. Phys.* **2000**, *113*, 9901−9904.

https://dx.doi.org/10.1021/acsami.0c12437
ACS Appl. Mater. Interfaces 2020, 12, 39352−39361

(51) Perdew, J. P.; Burke, K.; Ernzerhof, M. Generalized Gradient Approximation Made Simple. *Phys. Rev. Lett.* **1996**, *77*, No. 3865.
(52) Dunphy, J. C.; Rose, M.; Behler, S.; Ogletree, D. F.; Salmeron, M.; Sautet, P. Acetylene Structure and Dynamics on Pd(111). *Phys. Rev. B* **1998**, *57*, No. R12705.
(53) Pallassana, V.; Neurock, M.; Lusvardi, V. S.; Lerou, J. J.; Kragten, D. D.; Van Santen, R. A. A Density Functional Theory Analysis of the Reaction Pathways and Intermediates for Ethylene Dehydrogenation over Pd(111). *J. Phys. Chem. B* **2002**, *106*, 1656−1669.
(54) Medlin, J. W.; Allendorf, M. D. Theoretical Study of the Adsorption of Acetylene on the (111) Surfaces of Pd, Pt, Ni, and Rh. *J. Phys. Chem. B* **2003**, *107*, 217−223.
(55) Sheth, P. A.; Neurock, M.; Smith, C. M. First-Principles Analysis of Acetylene Hydrogenation over Pd(111). *J. Phys. Chem. B* **2003**, *107*, 2009−2017.
(56) Yang, L.; Guo, Y.; Long, J.; Xia, L.; Li, D.; Xiao, J.; Liu, H. PdZn Alloy Nanoparticles Encapsulated within a few Layers of Graphene for Efficient Semi-Hydrogenation of Acetylene. *Chem. Commun.* **2019**, *55*, 14693−14696.
(57) Sutter, P.; Sadowski, J. T.; Sutter, E. A. Chemistry Under Cover: Tuning Metal-Graphene Interaction by Reactive Intercalation. *J. Am. Chem. Soc.* **2010**, *132*, 8175−8179.
(58) Mu, R.; Fu, Q.; Jin, L.; Yu, L.; Fang, G.; Tan, D.; Bao, X. Visualizing Chemical Reactions Confined Under Graphene. *Angew. Chem., Int. Ed.* **2012**, *51*, 4856−4859.
(59) Ma, L.; Zeng, X. C.; Wang, J. Oxygen Intercalation of Graphene on Transition Metal Substrate: An Edge-Limited Mechanism. *J. Phys. Chem. Lett.* **2015**, *6*, 4099−4105.
(60) Wong, K.; Kang, S. J.; Bielawski, C. W.; Ruoff, R. S.; Kwak, S. K. First-Principles Study of the Role of O_2 and H_2O in the Decoupling of Graphene on Cu(111). *J. Am. Chem. Soc.* **2016**, *138*, 10986−10994.
(61) Locatelli, A.; Santos, B.; Vlaic, S.; Rougemaille, N.; Coraux, J.; Kimouche, A. Cobalt Intercalation at the Graphene/Iridium(111) Interface: Influence of Rotational Domains, Wrinkles, and Atomic Steps. *Appl. Phys. Lett.* **2014**, *104*, No. 101602.
(62) Zhang, Y.; Weng, X.; Li, H.; Li, H.; Wei, M.; Xiao, J.; Liu, Z.; Chen, M.; Fu, Q.; Bao, X. Hexagonal Boron Nitride Cover on Pt(111): A New Route to Tune MoleculeMetal Interaction and Metal-Catalyzed Reactions. *Nano Lett.* **2015**, *15*, 3616−3623.
(63) Sun, M.; Fu, Q.; Gao, L.; Zheng, Y.; Li, Y.; Chen, M.; Bao, X. Catalysis under shell: Improved CO oxidation reaction confined in Pt@h-BN core-shell nanoreactors. *Nano Res.* **2017**, *10*, 1403−1412.
(64) Khan, N. A.; Shaikhutdinov, S.; Freund, H. J. Acetylene and Ethylene Hydrogenation on Alumina Supported Pd-Ag Model Catalysts. *Catal. Lett.* **2006**, *108*, 159−164.
(65) Pachulski, A.; Schödel, R.; Claus, P. Performance and Regeneration Studies of Pd-Ag/Al_2O_3 Catalysts for the Selective Hydrogenation of Acetylene. *Appl. Catal., A* **2011**, *400*, 14−24.
(66) Huang, D.; Chang, K.; Pong, W.; Tseng, P.; Hung, K.; Huang, W. Effect of Agpromotion on Pd Catalysts by XANES. *Catal. Lett.* **1998**, *53*, 155−159.
(67) Praserthdam, P.; Ngamsom, B.; Bogdanchikova, N.; Phatanasri, S.; Pramotthana, M. Effect of the Pretreatment with Oxygen and/or Oxygen-containing Compounds on the Catalytic Performance of Pd-Ag/Al_2O_3 for Acetylene Hydrogenation. *Appl. Catal., A* **2002**, *230*, 41−51.
(68) Wang, A.; Li, J.; Zhang, T. Heterogeneous Single-Atom Catalysis. *Nat. Rev. Chem.* **2018**, *2*, 65−81.
(69) Giannakakis, G.; Flytzani-Stephanopoulos, M.; Sykes, E. C. H. Single-Atom Alloys as a Reductionist Approach to the Rational Design of Heterogeneous Catalysts. *Acc. Chem. Res.* **2019**, *52*, 237−247.

https://dx.doi.org/10.1021/acsami.0c12437
ACS Appl. Mater. Interfaces 2020, 12, 39352−39361